ARTICLE NO. 78-380R

Vapor Flow Calculations in a Flat-Plate Heat Pipe

H. van Ooijen* and C. J. Hoogendoorn†
Delft University of Technology, Delft, The Netherlands

Steady laminar incompressible two-dimensional flow in a horizontal flat plate heat pipe with an adiabatic top plate was studied. For uniform evaporation and condensation rates, the Navier-Stokes equations and the continuity equation were solved. For radial Reynolds numbers $Re_r > 1$, the velocity profiles were nonsimilar and asymmetrical. At $Re_r > 10$, backflow was observed along the top plate, starting at the end of the condensation zone. At the highest $Re_r (= 50)$, the total pressure drop over the heat pipe was more than three times the value found from Poiseuille approximation. However, complete recovery of impulse pressure was found and the additional pressure losses could be fully attributed to increased frictional losses. Experiments with a porous-plate model showed excellent agreement.

Nomenclature

D = thickness of heat pipe
k = pressure recovery factor
L = length of heat pipe, $L = L_e + L_a + L_c$
L_a = length of adiabatic zone
L_c = length of condensation zone
L_e = length of evaporation zone
L_{eff} = effective length, $L_{\text{eff}} = \frac{1}{2}L_e + L_a + \frac{1}{2}L_c$
p = pressure
p_i = impulse pressure defined in Eq. (9)
p_f = frictional pressure defined in Eq. (10)
δp = pressure drop according to Poiseuille flow approximation
Δp = total pressure drop
R = pipe radius
Re_a = Reynolds number in adiabatic zone, $Re_a = 2\rho \bar{u}_a D/\mu$
Re_r = radial Reynolds number, $Re_r = \rho v_0 D/\mu$
u, v = velocity components in x, y direction
v_0 = injection and suction v velocity
$\bar{u}_a$ = average u velocity in adiabatic zone
x, y = Cartesian coordiantes
μ = viscosity
ρ = density

Introduction

NEAR the low-temperature operating limit of a heat pipe, its capacity is influenced by the viscous and inertia forces in the vapor flow. The recirculation of fluid within a heat pipe is caused entirely by the presence of a pressure difference. This pressure difference is generated by the temperature difference present in the vapor along the heat pipe and acts as the driving force for the vapor flow overcoming the losses in vapor and liquid flow.

There have been numerous theoretical investigations connected with the problem of vapor flow in a heat pipe. These are concerned mainly with steady, incompressible, axisymmetrical laminar flow with uniform injection and or suction. Many of these investigations are applicable to a part of the heat pipe only, rather than to a complete heat pipe structure. These are carried out with similarity profiles, perturbation techniques, series expansions, transformation techniques, and numerical methods.

The foremost theoretical investigator of the heat pipe, Cotter,[1] has used the results obtained by Yuan and Finkelstein[2] for values of the radial Reynolds number $Re_r \ll 1$. The expression used for the evaporator pressure drop is presented in the form of a series expansion with Re_r as parameter. The results show that for this range of Reynolds values, the pressure profile is very close to the one that can be obtained by integration of the Poiseuille flow equation. For values of $Re_r \gg 1$, Cotter has used the pressure gradients obtained by Knight and McInteer.[3] He examined the evaporation and condensation zones separately. From the pressure profiles it was concluded that for high flow rates the impulse pressure recovery in the condensation zone is only partial and the recovered fraction k was found to be $k = 4/\pi^2$. This means that the total pressure drop in a heat pipe Δp would be much larger than based on viscous forces only.

Berman[4] has reported the effect of fluid withdrawal or injection on the flowfield in a pipe, a rectangular channel, and an annulus. He used perturbation solutions with Re_r as the parameter and found that fluid withdrawal has a much stronger effect on the pressure gradients and velocity profiles than has fluid injection. These effects are stronger for pipe flow than for channel flow. His numerical solutions for pipe flow provide no results for $2.3 < Re_r < 9.1$, indicating that for these values, nonsimilar profiles with flow reversal at the walls will occur in the condensation zone.

Terrill and Thomas[5] gave a complete analysis of the laminar flow through a uniformly porous pipe with injection and suction. With a numerical integration procedure they found dual solutions over the complete range of Re_r values, except for the range where Berman could not find any solutions either, $2.3 < Re_r < 9.1$. Additional solutions for both small and large Re_r values were generated by perturbation techniques, and coincided with the numerical results.

Quaile and Levy[6] have carried out theoretical and experimental investigations on the flow in a porous tube with wall suction. The study was confined to steady, laminar, incompressible flow with a parabolic velocity profile at the entrance of the "wall suction" section of the pipe. Solutions were found by expanding the stream function in a power series, followed by numerical integration. The analysis predicts regions of zero wall shear stress and flow reversal for $Re_r > 2.5$. In their experimental results, it is shown that the regions of reverse flow are unstable and undergo transition to turbulence.

Presented as Paper 78-380 at the AIAA Third International Heat Pipe Conference, Palo Alto, Calif., May 22-24, 1978; submitted June 27, 1978; revision received May 20, 1979.

Index categories: Heat Pipes; Viscous Nonboundary-Layer Flows; Computational Methods.

*Research Scientist, Physics Dept., Heat Transfer Section. Member AIAA.

†Professor, Physics Dept., Heat Transfer Section.

Busse[7] has considered the problem of pressure drop in the laminar vapor flow in a long, cylindrical heat pipe. He assumes a modified Poiseuille velocity profile. This analysis leads to similarity profiles for the evaporation zone. In the adiabatic zone, an exponential decay from the similarity profiles toward the Poiseuille profile is found. In the condensation zone, the profiles vary with the distance along the axis. The main limitation of Busse's work is that it ignores any backward influence on flow, which, in reality does exist. The important outcome of his analysis is that the total vapor pressure drop Δp along the heat pipe can be found by using the simple Poiseuille flow model for $Re_r < 1$.

Only a few investigators consider the complete heat pipe problem. Two-dimensional analysis of a cylindrical heat pipe is reported by Bankston and Smith.[8] For the case of laminar flow, the mass and momentum equations are solved with a finite-difference computation method based on the stream function-vorticity approach, thus eliminating the pressure as a separate variable. Results are reported over the range of $0.01 \leq Re_r \leq 1000$. For different ranges of Re_r values, the convergence and accuracy of the method depended largely on the appropriate choice of the vorticity boundary conditions for each particular range. With increasing Re_r values, deviations from the Poiseuille flow become evident first in the condenser. Flow reversal is encountered for $Re_r > 2$. In relative long heat pipes with equal evaporator and condenser lengths, the computed results for the total pressure drop agreed reasonably well with Busse's formula for $Re_r \leq 10$, in spite of the observed flow reversal. For length-to-radius ratios (L/R) of 400 and 40, the agreement was within 10% for $Re_r = 10$; however, for $L/R = 10$, the computed pressure drop was about 50% higher, thus indicating the influence of the end effects for a short heat pipe.

The authors have solved the problem of the two-dimensional flat-plate-type heat pipe with an adiabatic top wall using the same method. For $Re_r > 3$, the longitudinal pressure profiles at different heights did not match, resulting in a discrepancy with the calculated transverse pressure gradients. Though the velocity profiles at even higher Re_r values converged rapidly, the method was considered as unreliable due to the approximations at the vorticity boundary conditions and was therefore abandoned. To compare situations with pipe flow and parallel plate flow, it has to be noted that for pipe flow in the definition of Re_r, the radius R has to be used instead of the plate distance D. Lomax and Steger[9] have also indicated the difficulties connected with the stream function-vorticity method and show that for high Reynolds values, the convective terms dominate the equations. This complicates the iteration process in the relaxation methods, because truncation-error terms become predominant.

Tien and Rohani[10] also have used the stream function-vorticity method. In addition, they introduced the energy conservation equations and a thermodynamic equilibrium equation to couple the vapor pressure and the temperature. Results were obtained for radial Reynolds numbers up to 36 in the evaporation zone and 24 in the condensation zone. The overall pressure drop along the heat pipe in all cases was very close to the predictions of Busse, as based on the Poiseuille flow model. It was also demonstrated that solutions of the equations of the boundary-layer type provide accurate results for the vapor pressure distribution at low Re_r values only. From the results it is concluded that vapor pressure variations can play a significant role in the heat pipe performance.

Tien[11] has reviewed the fluid mechanical problems of heat pipes. For the vapor flow, the actual flowfield behavior differs from the basic flow regimes—creeping flow for low Reynolds numbers, entrance flow, and fully developed flow for higher Reynolds numbers—and this has not yet been studied in detail. He points out that the regions near the evaporator and condenser ends and the whole class of turbulent flows are some of the unexplored areas. The transition to turbulent flow at relative low Reynolds numbers due to wall suction and flow reversal needs further attention.

The literature review thus reveals that the complete problem of vapor flow in a heat pipe has been analyzed numerically by only a few investigators. Moreover, the computations with the pressure as a separate variable have not been reported so far. In the present paper, an analysis of the steady incompressible, two-dimensional laminar flow is presented for the case of a flat plate-type heat pipe with asymmetrical boundary conditions. The pressure term in the governing equations is retained as a separate variable.

Mathematical Formulation

Steady, incompressible, two-dimensional laminar flow in a horizontal flat plate heat pipe is considered. The schematic arrangement of the heat pipe under study is shown in Fig. 1. The top plate is assumed to be an adiabatic wall, so that the vapor flow becomes asymmetrical. The dimensions shown represent those of a heat pipe constructed in our laboratory that is used for the study of vapor flow and the evaporation and condensation behavior of water at about 20°C. This heat pipe has a transparent top plate to facilitate visual observations. The uniform inflow and outflow boundary conditions are referred to here as evaporation and condensation, respectively. No change of phase is actually involved in the calculations. Under these conditions, the continuity equation (1) and the momentum equations (2) and (3) govern the flow.

$$\frac{\partial u}{\partial x} + \frac{\partial v}{\partial y} = 0 \tag{1}$$

$$\rho u \frac{\partial u}{\partial x} + \rho v \frac{\partial u}{\partial y} = -\frac{\partial p}{\partial x} + \mu\left(\frac{\partial^2 u}{\partial x^2} + \frac{\partial^2 u}{\partial y^2}\right) \tag{2}$$

$$\rho u \frac{\partial v}{\partial x} + \rho v \frac{\partial v}{\partial y} = -\frac{\partial p}{\partial y} + \mu\left(\frac{\partial^2 v}{\partial x^2} + \frac{\partial^2 v}{\partial y^2}\right) \tag{3}$$

The boundary conditions of the problem are:

$$\begin{aligned}
&u(0,y) = v(0,y) = 0 \\
&u(L,y) = v(L,y) = 0 \\
&u(x,D) = v(x,D) = 0 \\
&u(x,0) = 0 \\
&v(x,0) = v_0 \qquad 0 \leq x \leq L_e \\
&v(x,0) = 0 \qquad L_e < x < (L_e + L_a) \\
&v(x,0) = -v_0 \qquad (L_e + L_a) \leq x \leq L \\
&p(0,0) = 0 \qquad \text{(assumed)}
\end{aligned} \tag{4}$$

A finite-difference procedure based on the computer program TEACH, developed by Gosman et al.[12] has been used. In this program, the finite-difference approximations to

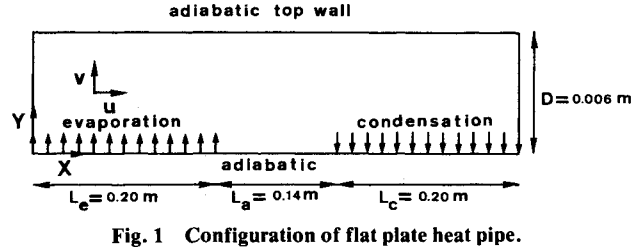

Fig. 1 Configuration of flat plate heat pipe.

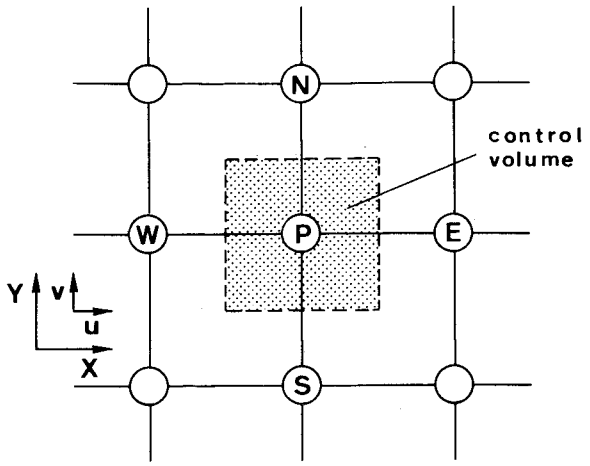

Fig. 2 General grid point locations.

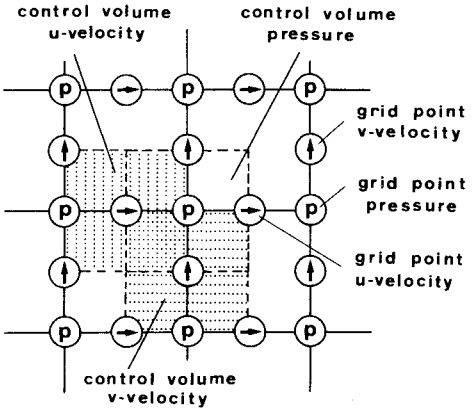

Fig. 3 Grid point locations for pressure and velocities.

the differential equations for the conservation of mass and momentum are expressed in a standard form:

$$\Sigma_i A_i \Phi_p = \Sigma_i A_i \Phi_i + S_p \tag{5}$$

where Φ is the general variable and the subscript i refers to the adjacent nodes of the point P, as illustrated in Fig. 2, namely, N,E,S, and W. For Φ the variables u,v, or p have to be filled in. The A_i's include both convective and diffusive transport and their exact form depends on the governing equation and the differential approach. The last term in Eq. (5) is a "source" term that may involve several effects that are typical for the particular problem. Three sets of equations of the type of Eq. (5) are used for the u velocity, the v velocity, and the pressure. Equations (2) and (3) are used for the u velocity and v velocity, respectively. In order to create an equation with the pressure p as the dependent variable, Eq. (1) is rewritten in the form:

$$\frac{\partial}{\partial x}\left(\Lambda_x \frac{\partial p}{\partial x}\right) + \frac{\partial}{\partial y}\left(\Lambda_y \frac{\partial p}{\partial y}\right) = 0 \tag{6}$$

where Λ_x and Λ_y stand for the "flow conductivity" in the x and y direction, respectively.

A "hybrid" difference scheme is used involving the combination of central and upwind difference techniques. The resulting equations are solved line by line by means of the tridiagonal matrix algorithm. The grid used in the procedure locates the pressures at the main grid nodes, while the velocities are located at displaced positions.

The three grids used for u,v, and p with their respective locations are shown in Fig. 3. In the present study, a nonlinear grid in the y direction is used with small increments near the walls, while in the x direction, the grid is uniform. A 19×28 point mesh is used, as shown in Fig. 4. In the table for Fig. 4, the exact locations of the grid points are given. The grid spacing near the walls in the y direction is about 1/20 that in the center to facilitate the study of steep velocity gradients that occur at the walls especially in the case of suction.

The steps involved in the calculation procedure can be summarized as follows:

1) Provide initial estimates of the values of velocities and pressures with the specified boundary conditions.

2) Solve the modified u momentum equation to obtain new values u', and solve the modified v momentum equation to obtain new values v' for the velocities.

3) Use the modified continuity equation using the updated values u' and v' and find the corrected values p' for the pressure.

4) Regard the new values as improved estimates, return to step 1 and repeat until convergence is reached.

The iteration process is monitored by comparing the sum of the absolute values of mass and momentum residues with set value criteria. Under-relaxation was used to reach a rapid and stable convergence. The computations were carried out on an IBM 370 computer of the Delft University. A core store capacity of 130 kbites was used. With increasing Re_r values, the number of iterations required to fulfill the set criteria of convergence increased sharply from about 30 for $Re_r = 1$ to 300 for $Re_r = 50$. As initial estimates for the values of the velocities and pressures, Poiseuille flow approximation results were used for $Re_r = 1$, while at higherRe_r values, the com-

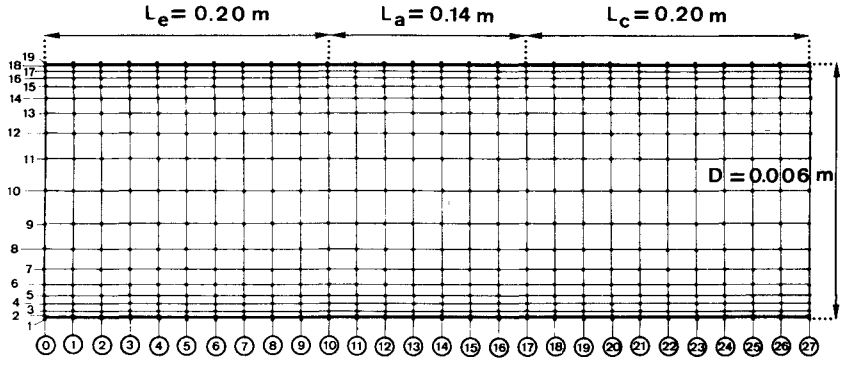

location nr	y-distance m
1	0.000000
2	0.000048
3	0.000171
4	0.000332
5	0.000541
6	0.000813
7	0.001167
8	0.001616
9	0.002223
10	0.003000

symmetrical non-linear y-grid locations

Fig. 4 Grid point configurations used with the computations.

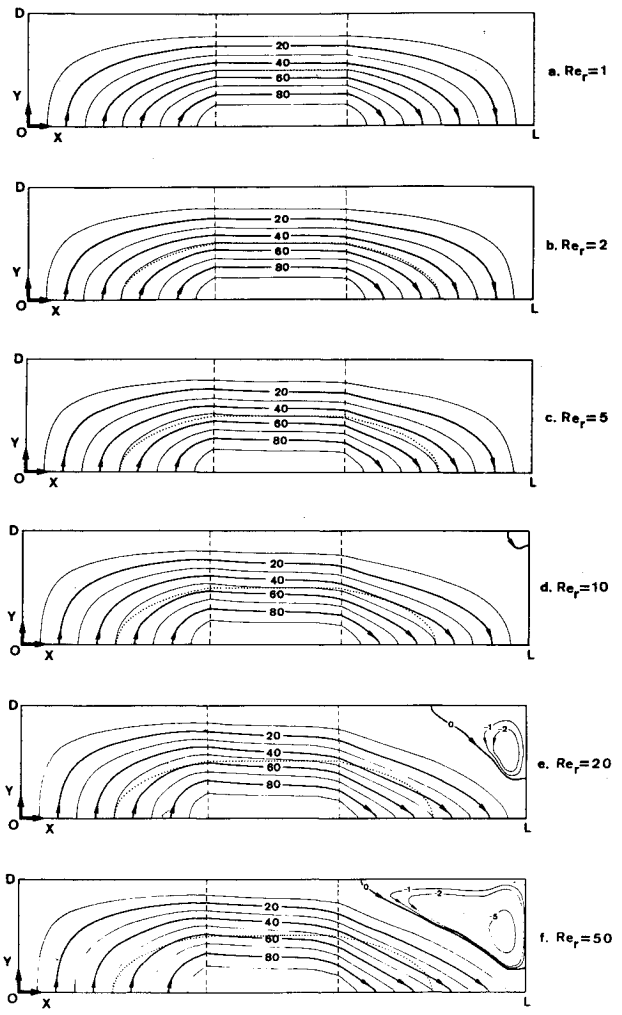

Fig. 5 Streamline plots for Re_r values 1, 2, 5, 0, 20, and 50.

putation results obtained at the preceding lower Re_r value were applied for this purpose. The maximum computation time required to reach convergence within 1% amounted to about 2 min for $Re_r = 50$.

Computation Results

A. Stream Functions

From the results of the computations, stream function values have been calculated for Re_r values of 1, 2, 5, 10, 20, and 50. The streamline plots are shown in Figs. 5a-f. For reason of space conservation, the x direction has been foreshortened more strongly than the y direction, giving a somewhat deformed picture. The uniform evaporation and condensation boundaries are clearly seen in all the streamline pictures. The normalized stream function values increase linearly from 0 to 100 along the evaporator, and decrease linearly from 100 to 0 along the condenser bottom wall. Along the bottom wall in the adiabatic zone, the stream function value remains constant at 100. The streamlines at the bottom wall in the evaporation and condensation zone are perpendicular to the wall, thus indicating the nature of these boundaries. The dotted curves show the streamlines with a normalized stream function value of 50 for $Re_r = 0.1$. For this low Re_r value, the viscous forces dominate and a modified Poiseuille flow model can be used to calculate the streamlines. This results in a symmetrical flow pattern for the evaporator and the condenser.

For $Re_r = 1$, no deviation of the streamlines from the Poiseuille flow model is observed. For $Re_r = 2$, the streamlines in the evaporator show a trend to move toward the adiabatic top wall, while in the condenser the opposite behavior is observed. In the adiabatic zone hardly any change can be seen at this Re_r value. For $Re_r = 5$, the deviations in the evaporator and the condenser become stronger, and in the entrance zone of the adiabatic part, a difference from the modified Poiseuille flow model is noticed. For $Re_r = 10$, a small recirculation zone appears near the top end corner in the condensation zone, which amounts to less than 0.2% of the total flow. For $Re_r = 20$, the wall separation point has moved upstream to halfway down the condenser and the recirculating flow cell is equal to more than 2% of the flow. At $Re_r = 50$, recirculation starts shortly after the flow enters the condensation zone and involves more than 5% of the flow. From the occurrence of recirculating zones in the computation results, it may be expected that transition from laminar to turbulent flow could be stimulated by these phenomena.

In the evaporation zone, the change in the flow pattern is less dramatic, though an increased shifting of the flow lines toward the adiabatic top plate is clearly observed with increasing Re_r values.

In the adiabatic zone it is seen that the flow lines remain parallel to the walls only at low Re_r values and, as a result, a complete decoupling between the flows in the evaporator and the condenser is present for these values only. In the entrance of the adiabatic zone, an entrance effect caused by the evaporation zone flow distortion decays fast at low Re_r values. This effect persists for higher Re_r values until at $Re_r = 10$ the influences of the evaporation zone and the condensation zone meet near the end of the adiabatic zone, thus giving a weak coupling between the flows in the evaporator and the condenser. For the decay length L_d of a flow disturbance in a rectangular channel, Brodkey[13] gives the formula:

$$L_d/D = 0.04\, Re_a \tag{7}$$

The decay length L_d is defined as the length required for the flow to change from a rectangular profile to a Poiseuille profile within 1% of the maximum velocity between two parallel plates at a distance D. Applying this formula to the present case for $Re_r = 10$, a decay length of 0.16 m in the adiabatic zone is obtained, which agrees nicely with our results in Fig. 5d.

At still higher Re_r values, the stream patterns in the evaporation and condensation zones becomes strongly coupled. This fact leads to the important conclusion that any calculation that denies this coupling will lead to wrong results. It can further be stated that the adiabatic section of the heat pipe has a specific influence on the heat pipe performance, and thus is more than a junction piece between evaporator and condenser because of the vapor flow decoupling effect at low Re_a values.

B. Velocities

Figures 6a-c show the dimensionless u velocity profiles across the transverse sections in the evaporator zone for Re_r values of 2, 10, and 50. For comparison, parabolic Poiseuille profiles are also plotted as dotted lines for three locations in the same figures. For $Re_r = 2$ the profiles differ very little from the Poiseuille profiles, indicating the strong dominance of viscous forces. From the constant shape, it can be concluded that these are similarity profiles; the velocity maxima have been shifted toward the top wall and reveal the asymmetric boundary conditions. With increasing Re_r values, the shifting proceeds continuously, giving an increase in the wall shear stresses at the top wall and a decrease at the bottom wall. For small Re_r values, this net effect is small compared to the undisturbed shear stress values; for larger Re_r values, a marked effect on the pressure gradients will result. For $Re_r = 50$, the profiles still basically show similarity, but reveal

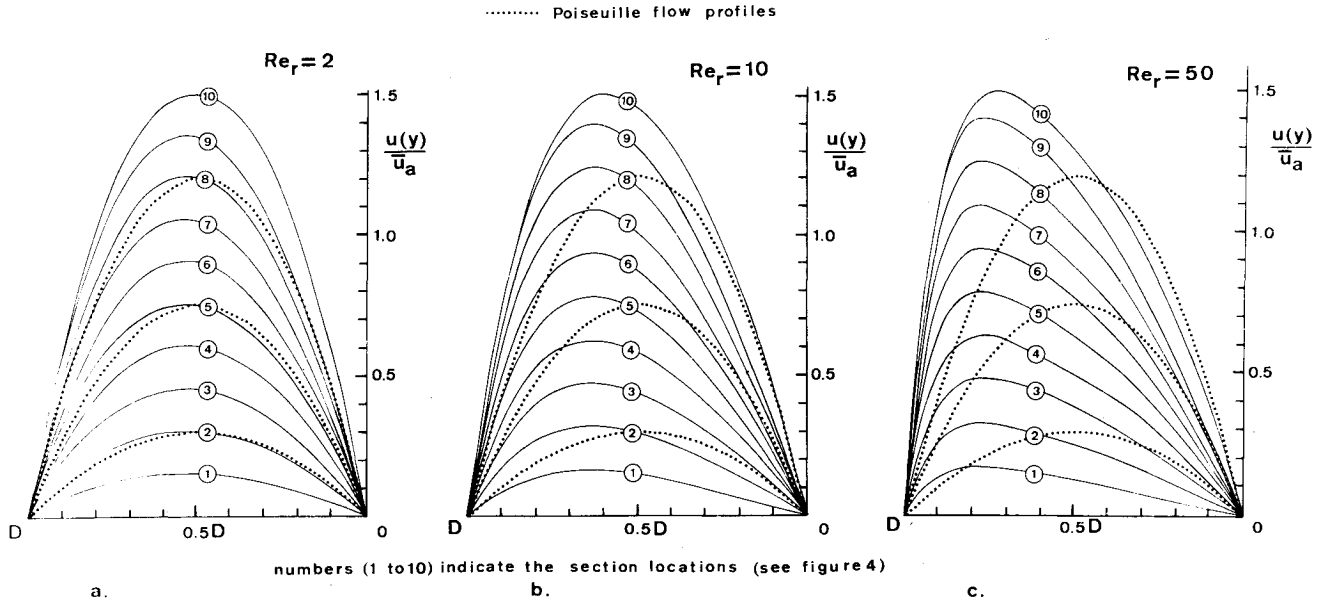

Fig. 6 Dimensionless u velocity profiles along the evaporator cross sections.

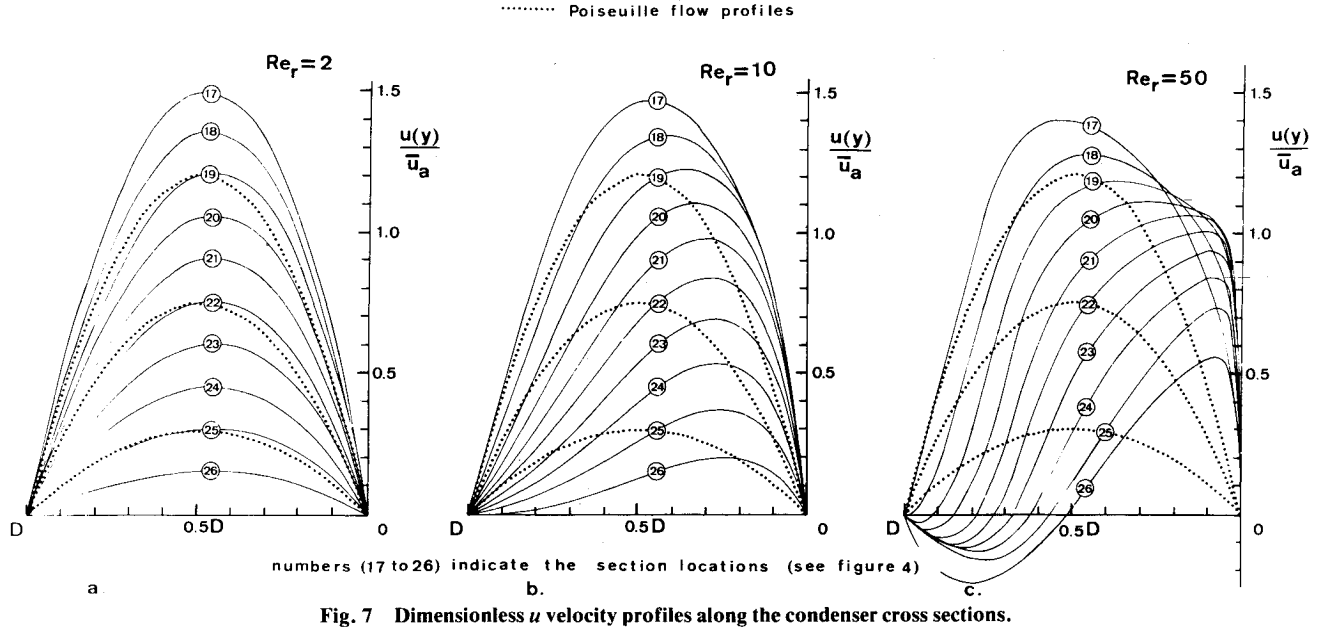

Fig. 7 Dimensionless u velocity profiles along the condenser cross sections.

a changing nature along the evaporator due to entrance effects, and complete similarity no longer exists. At $x=0.20$ m the velocity profiles are different because of the changeover in the boundary conditions occurring at this location.

Figures 7a-c show the u-velocity profiles over the condenser section for Re_r values of 2, 10, and 50. At the lowest value of $Re_r=2$, there is already a marked deviation from similarity profiles, as can be seen from the continuous shifting of the velocity maxima along the length of the condenser. At equal Re_r values, the deviation from the Poiseuille profile in the condenser is much larger than in the evaporator.

Inflection points in the velocity profiles are observed for $Re_r \geq 2$, indicating an inherent instability leading to separation and regions of reversed flow. For $Re_r=10$, flow reversal takes place at the top end of the condenser where the suction effects are least felt (see Fig. 5d). The velocity profile at $x=0.52$ m—the last grid point before the end wall—shows the separation point with zero wall shear stress. At still higher values of Re_r, this point of zero wall shear stress moves upstream. In combination herewith, the zone with reversed flow increases with increasing Re_r values. At $Re_r=50$, zero wall shear stress is found at the first grid point in the condensation zone and flow reversal is present at all locations. At this high Re_r value, backflow with velocities of nearly 50% of the forward ones occur. The very steep velocity gradients present at the bottom wall result in a tremendous increase in local wall shear stresses at this boundary. For $Re_r=2$, the local wall shear stresses throughout the condensation zone are about 1.5 times the values resulting from the undisturbed Poiseuille flow. For $Re_r=10$ this ratio increases from 2.5 at the entrance of the condensation zone to 3.8 near the end. At the highest Re_r value shown, $Re_r=50$, this shear stress ratio varies from 6.5 at the entrance to 40 at the end of the condenser, indicating clearly that the flow is dominated by the inertia forces.

For the adiabatic zone, no velocity profiles are shown. However, the computations show that for very low Re_r values, the undisturbed Poiseuille profile results. The deviation from the Poiseuille flow depends on both the Re_r value and the value of the axial Reynolds number in the

adiabatic zone, Re_a. The deviation at the entrance of the adiabatic zone increases with increasing Re_r values; the decay length of the deviation depends on Re_a. For $Re_r > 10$, a continuous changing profile is observed throughout the adiabatic zone. This is in agreement with the predictions of the decay length given by Eq. (7) and results in a direct coupling between the evaporator and condenser flows.

C. Pressure

Longitudinal pressure gradients along a heat pipe represent a combined effect of an impulse term and a term due to frictional effects:

$$\frac{dp(x)}{dx} = \frac{dp_i(x)}{dx} + \frac{dp_f(x)}{dx} \tag{8}$$

Both terms contribute over the evaporator and condenser zones, while frictional effects mainly contribute over the adiabatic region. Assuming constant pressure over a cross section, the impulse pressure term $p_i(x)$ is defined equal to the average momentum flux over the cross section:

$$p_i(x) = \frac{1}{D}\int_0^D \rho u^2 dy = \rho \overline{u^2} \tag{9}$$

The term in the pressure gradient due to wall friction is equal to the sum of the shear stresses at the top and bottom wall:

$$\frac{dp_f(x)}{dx} = -\mu \left.\frac{\partial u}{\partial y}\right|_{y=0}^{y=D} \tag{10}$$

If Poiseuille profiles are assumed for the u velocity in the y direction, the impulse pressure loss resulting from the flow acceleration in the evaporator is:

$$p_i(x) = -6\rho \bar{u}_a^2 x^2 / 5L_e^2 \tag{11}$$

In the adiabatic zone there is no contribution from the inertial term if the flow profile remains constant. In the condensation zone, a complete recovery of the pressure loss in the evaporator takes place due to the flow deceleration:

$$p_i(x) = -\frac{6\rho \bar{u}_a^2 (L-x)^2}{5L_c^2} \tag{12}$$

This results in a value $k = 1$ for the impulse pressure recovery.

The frictional pressure drop over the heat pipe can be estimated by integrating the Poiseuille flow pressure gradient. In the evaporation zone, the average u velocity increases linearly with x, which gives a quadratic pressure profile:

$$p_f(x) = p_f(0) - 6\mu \bar{u}_a x^2 / D^2 L_e \tag{13}$$

In the adiabatic zone, the average u velocity is constant $\bar{u}_a$ and, as a result, a linear pressure profile is found in this zone:

$$p_f(x) = p_f(L_e) - 12\mu \bar{u}_a x / D^2 \tag{14}$$

In the condensation zone, the average u velocity decreases linearly, which results in the quadratic pressure profile:

$$p_f(x) = p_f(L) + \frac{6\mu \bar{u}_a (L-x)^2}{D^2 L_c} \tag{15}$$

The total pressure drop δp over the heat pipe for the case of Poiseuille flow approximation results from the addition of the separate contributions:

$$\delta p = 12\mu \bar{u}_a L_{\text{eff}} / D^2 \tag{16}$$

in which L_{eff} is the effective heat pipe length.

$$L_{\text{eff}} = \tfrac{1}{2}L_e + L_a + \tfrac{1}{2}L_c \tag{17}$$

From Eqs. (11) and (13), it follows that the ratio of the impulse and the frictional pressure gradient in the evaporator section will be proportional to the radial Reynolds number:

$$\frac{dp_i(x)}{dx} \Big/ \frac{dp_f(x)}{dx} = \frac{1}{5} Re_r \tag{18}$$

In the condenser section, the contributions have an opposite sign. This results in a constant pressure in this section for a radial Reynolds number equal to 5. For even higher Re_r values, the impulse pressure term becomes dominant and a pressure buildup will result in the condenser.

It will be clear that only for low Re_r values is the Poiseuille flow approximation valid. With increasing Re_r values, the velocity profiles start to deviate from the Poiseuille flow behavior, as can be seen from Figs. 6 and 7. This results in an increase of both frictional and impulse pressure losses in the evaporator. At high Re_r values, the impulse pressure term becomes important, even in the adiabatic zone because of the continuous change in the velocity profiles.

In the condensation zone, the frictional losses become very high, especially in the cases of flow reversal for $Re_r > 10$. Under these conditions, Eq. (16) is no longer valid and the total pressure drop Δp is significantly larger than the Poiseuille flow approximation pressure drop δp. The main reason for this is found in the asymmetric boundary conditions. A formula similar to Eq. (16) has been introduced by Busse for the total pressure drop in a cylindrical heat pipe; he did not use the Poiseuille approximation.

In Fig. 8 the variation of the longitudinal pressure drop is plotted in the dimensionless form $p/\delta p$ for Re_r values of 1, 2, 5, 10, 20, and 50. Even for the highest Re_r value shown in the figure, the transverse pressure differences are so small that a single graph can be used to represent the longitudinal pressure variation for all y values. For small values of Re_r, the pressure profile is close to the Poiseuille flow model, as can be seen from the dotted line for $Re_r = 1$. For $Re_r = 2$, the computed total pressure drop Δp is only 1% higher than δp, revealing the dominance of viscous forces. For $Re_r = 5$, a constant pressure is found in the condenser section, while at still higher Re_r values a pressure buildup is seen, as could be expected from Eq. (18). At the highest Re_r value shown, $Re_r = 50$, the total pressure drop Δp is more than three times the pressure drop δp resulting from Eq. (16). This is mainly caused by the

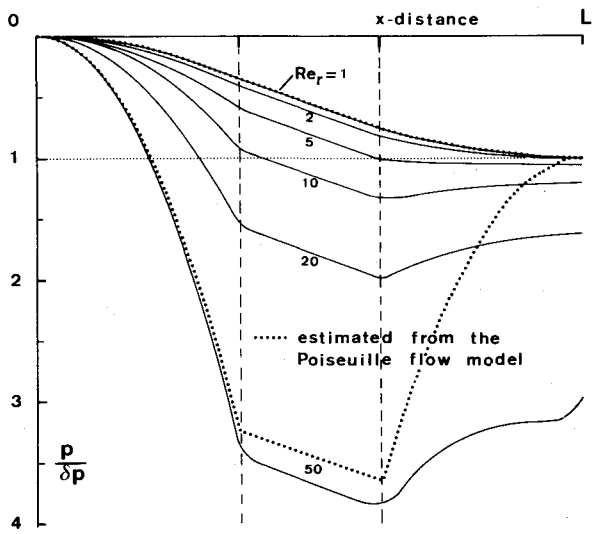

Fig. 8 Longitudinal pressure variation.

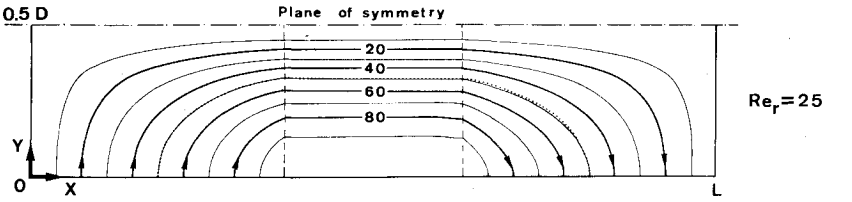

Fig. 9 Streamline plots for $Re_r = 25$ with symmetrical boundary conditions.

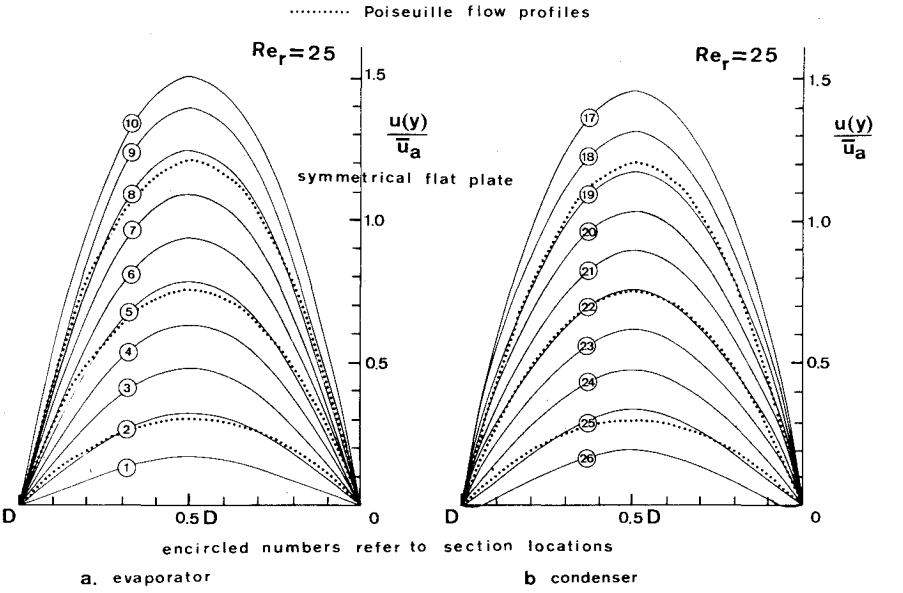

Fig. 10 Dimensionless u velocity profiles along the evaporator and condenser cross sections, symmetrical case.

flow pattern in the condenser, as can be concluded from the large deviation from the Poiseuille flow model in this section shown in Fig. 5. The sharp pressure increase at the end of the condensation zone is attributed to the recirculation.

In order to study the contributions of frictional and impulse pressure losses in the heat pipe, both terms were computed separately for $Re_r = 50$.

From the velocity profiles, the impulse pressure term along the heat pipe was calculated using Eq. (9). A complete impulse pressure recovery, $k = 1$, was found, as expected, for a complete heat pipe. Integration of the wall shear stresses along the heat pipe revealed that in the condenser section, the friction losses could not be neglected, as expected from Eq. (15), but remained of roughly equal importance as the impulse pressure term even at this high Re_r value. Our computations revealed appreciable transverse pressure gradients at both ends of the adiabatic zone, causing the changes in the u-velocity profiles at these locations. The transverse pressure gradient is dominant near the entrance of the condensation zone, because the local pressure gradient in the x direction goes through zero for $Re_r > 5$. Even there, however, the actual transverse pressure difference in the y direction remains negligibly small because of the short y distance involved.

In most of the theoretical articles, the effect of transverse pressure gradients is neglected and "open end" type calculations are used for the flow profiles in the evaporator and condenser. This leads to erroneous results, especially at higher Re_r values. Cotter's impulse pressure recovery factor $k = 4/\pi^2$ is also based on such calculations.

Symmetrical Flow

For comparison, computations were carried out for the symmetrical case with evaporation and condensation on both the top and bottom plates of the heat pipe. The geometrical configuration of the heat pipe was kept unchanged. To compare flow situations with equal axial flow, the Re_r value for the symmetrical case should be chosen at half the value of the asymmetrical case. In Fig. 9, a typical streamline pattern is shown for $Re_r = 25$. This flow pattern has to be compared with Fig. 5f for conditions of equal total flow. For a better comparison, the y dimensions in Fig. 9 are enlarged twice as compared to Fig. 5f, and only half of the streamline plots are presented. In the evaporation zone, the flow is nearly undisturbed despite the high Re_r value. In the condensation zone, a very small flow distortion is observed.

Figure 10a shows the u velocity profiles in the evaporator for $Re_r = 25$. The flow injection at the walls results in the cosine similarity profiles in agreement with the work of Knight and McInteer. However, the difference between the cosine profile and the Poiseuille profile is not very large. In Fig. 10b, the profiles over the condenser section are shown. At this high Re_r value, small regions with flow reversal are present at the far end corners. The effect of wall suction results in steep velocity gradients at the walls in the first part of the condenser. The flow reversal at the far end produces low wall shear stresses in that region. This results in a changeover of the velocity profiles near the end of the zone. In Fig. 11, the dimensionless u velocity profiles for $Re_r = 25$ at three transverse sections in the condenser are compared with the profiles as obtained by Knight and McInteer for $Re_r = 21.3$ and 38.5. Their results were based on numerical integration in a condenser of semi-infinite length, assuming similarity profiles, equivalent to the condition of zero transverse pressure gradients. This leads to uniform dimensionless u velocity profiles throughout the condenser that are much more flat than ours. The difference between the results indicate the limited value of calculations based on assumptions such as zero transverse pressure gradients.

Figure 12 shows the variation of the longitudinal dimensionless pressure for Re_r values of 5 and 25. Even at the highest Re_r value of 25, the pressure profile does not deviate significantly from the prediction based on the Poiseuille flow approximation, and the total pressure drop over the heat pipe is only 10% larger than calculated from Eq. (16). This clearly indicates that the velocity gradients at the evaporator and condenser boundaries remain close to their values based on

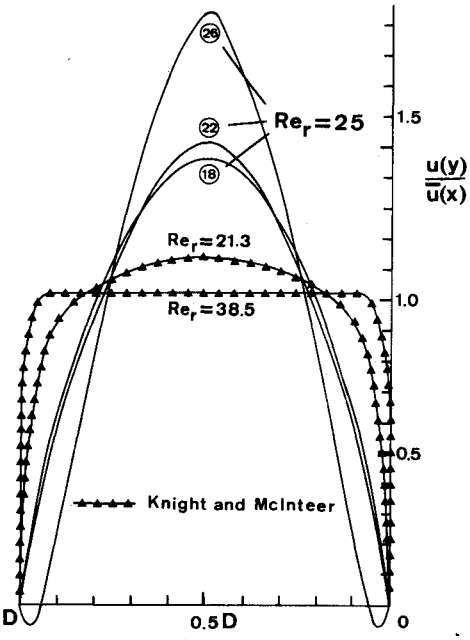

Fig. 11 Comparison of dimensionless u velocity profiles in the condenser with results of Knight and McInteer.

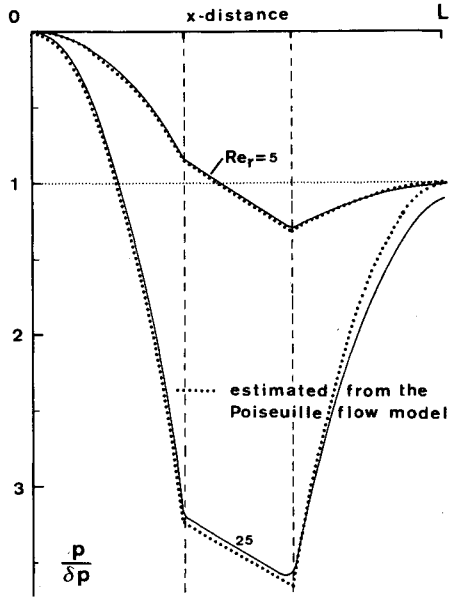

Fig. 12 Pressure distribution for symmetrical case.

the Poiseuille flow model. Though flow reversal takes place, there is no indication of a recirculation zone that caused the large increase in frictional losses in the asymmetrical case.

Our results were obtained for relatively long heat pipes with a L/D ratio of 90. Results for a smaller L/R ratio, as reported by Bankston and Smith for pipe flow, show that for $L/R = 10$, the end effects become very important for $Re_r > 10$, as an exceptional increase in their total pressure drop occurred beyond this value.

Comparison with Experiments

An experimental setup was made, as shown schematically in Fig. 13. The dimensions were kept equal to those of the theoretical model used in the computations. The channel width was chosen as 0.06 m to have a nearly two-dimensional flow situation. The flow conditions of uniform evaporation and condensation were simulated by uniform injection and removal of nitrogen gas through the porous bottom walls of

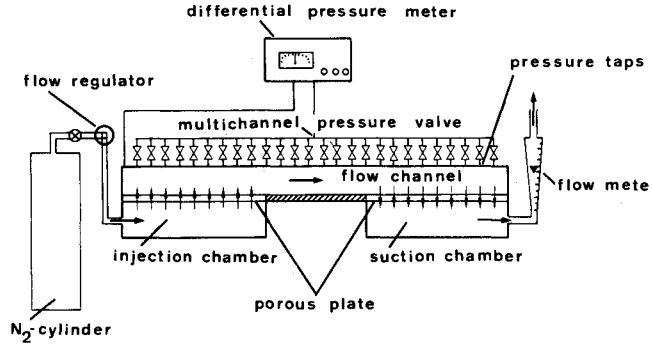

Fig. 13 Asymmetric experimental setup.

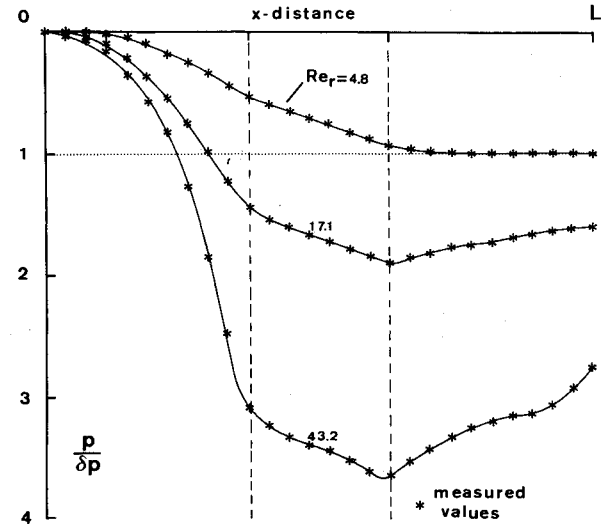

Fig. 14 Experimental pressure distributions.

the evaporator and condenser sections. The porous bottom plate was made of sintered stainless steel having a porosity of 40 μm and a thickness of 1.6 mm. The bottom plate was sealed over the adiabatic zone. The gas flow rate was measured by a variable area flowmeter. In the top plate, 28 pressure taps were located at equal intervals of 0.02 m. The pressure differences between the locations were measured with a micromanometer by means of a multichannel valve. The full-scale sensitivity of the micromanometer was 1 N/m^2.

Pressure profiles were measured over the range of Re_r values between 4.8 and 43.2. In Fig. 14, the dimensionless longitudinal pressure distributions at the top plate are shown for three typical Re_r values. The dimensionless pressures are presented as the ratio of the actual pressure drop to the pressure drop δp based on Poiseuille flow approximation. At the low Re_r value of 4.8 the pressure decreases quadratically over the evaporator, linearly over the adiabatic zone, and remains practically constant over the condenser zone, as expected theoretically. The total pressure drop Δp is equal to δp.

With increasing Re_r values, the pressures become significantly affected by the additional friction effects resulting from flow distortion, especially in the condenser section. At $Re_r = 17.1$, the ratio of the actual pressure drop Δp and the value based on the Poiseuille flow approximation δp is already 1.6. Halfway in the condenser section, a small distortion of the pressure profile can be noticed. This is assumed to be the result of flow reversal. For the highest experimental value of Re_r that could be obtained, $Re_r = 43.2$, the pressure drop ratio is 2.8 and a sharp increase of pressure in the hindmost part of the condenser reveals a strong flow recirculation in agreement with the numerical results. In

conclusion, it can be said that there is a good qualitative and quantitative agreement between the experimental pressure profiles and those resulting from the computations as plotted in Fig. 8.

Conclusions

The computation program TEACH from Gosman et al. has been used successfully to solve the velocity and pressure profiles in a flat plate heat pipe with laminar flow with both symmetrical and asymmetrical boundary conditions. For the symmetrical case, the computed value of the total pressure drop over the heat pipe Δp was practically equal to the prediction, based on a modified Poiseuille flow model for radial Reynolds values $Re_r \leq 25$.

For the asymmetrical case, Δp was much larger than followed from this model. This is due to the generation of a recirculating flow zone in the condenser that causes very steep velocity gradients and a tremendous increase in wall shear stresses in this section for $Re_r \geq 10$. In the symmetrical case, flow reversal and wall separation were observed, but the formation of a recirculating flow cell is prevented by the suction boundaries.

In all computational results, the pressure recovery of the impulse term was complete, i.e., $k=1$. It is shown that a separate treatment of evaporator and condenser flows leads to wrong results at high Re_r values. Only for low Re_r values is a complete decoupling of the flows present. Therefore, Cotter's impulse pressure recovery factor $k=4/\pi^2$ cannot be used to predict pressure drops in a complete heat pipe.

Acknowledgment

The authors are most grateful to N. K. Sane, who assisted with the computations and preparation of the manuscript.

References

[1] Cotter, T. P., "Theory of Heat Pipes," Los Alamos Scientific Lab., Rept. LA-3246-MS, 1965.

[2] Yuan, S. W. and Finkelstein, A. B., "Laminar Flow with Injection and Suction Through Porous Walls," *Transactions of ASME*, Vol. 78, 1956, pp. 719-724.

[3] Knight, B. W. and McInteer, B. B., "Laminar Incompressible Flow in Channels with Porous Walls," LADC-5309.

[4] Berman, A. S., "Effect of Porous Boundaries on the Flow of Fluids in Systems with Various Geometries," *Proceedings of the International Conference of Peaceful Use of Atomic Energy*, Vol. 4, 1958, pp. 351-358.

[5] Terrill, R. M. and Thomas, P. W., "On Laminar Flow Through a Uniformly Porous Pipe," *Applied Science Research*, Vol. 21, 1969, pp. 37-67.

[6] Quaile, J. P. and Levy, E. K., "Laminar Flow in a Porous Tube with Suction," *Transactions of ASME Journal of Heat Transfer*, Vol. 97, 1975, pp. 66-71.

[7] Busse, C. A., "Pressure Drop in the Vapor Phase of Long Heat Pipes," Thermionic Conversion Specialist Conference, 1967, pp. 391-398.

[8] Bankston, C. A. and Smith, H. J., "Vapor Flow in Cylindrical Heat Pipes," *Transactions of ASME, Journal of Heat Transfer*, Vol. 95, 1973, pp. 371-376.

[9] Lomax, H. and Steger, J. L., "Relaxation Methods in Fluid Mechanics," *Annual Review of Fluid Mechanics*, Vol. 7, 1975, pp. 63-88.

[10] Tien, C. L. and Rohani, A. R., "Analysis of the Effects of Vapor Pressure Drop on Heat Pipe Performance," *International Journal of Heat Mass Transfer*, Vol. 17, 1974, pp. 61-67.

[11] Tien, C. L., "Fluid Mechanics of Heat Pipes," *Annual Review of Fluid Mechanics*, Vol. 7, 1975, pp. 167-185.

[12] Gosman, A. D., Pun, W. M., and Spalding, D. B., Lecture Notes for Course Entitled "Calculation of Recirculating Flows," Imperial College, London, HTS/74/2, 1974.

[13] Brodkey, R. S., *The Phenomena of Fluid Motions*, Addision-Wesley Publishing Co., Calif., 1967, p. 129.